JACS
JOURNAL OF THE AMERICAN CHEMICAL SOCIETY
Article
pubs.acs.org/JACS

Interlocked Catenane-Like Structure Predicted in $Au_{24}(SR)_{20}$: Implication to Structural Evolution of Thiolated Gold Clusters from Homoleptic Gold(I) Thiolates to Core-Stacked Nanoparticles

Yong Pei,*[,†] Rhitankar Pal,[‡] Chunyan Liu,[†] Yi Gao,[‡] Zhuhua Zhang,[§] and Xiao Cheng Zeng*[,‡]

[†]Department of Chemistry, Key Laboratory of Environmentally Friendly Chemistry and Applications of Ministry of Education, Xiangtan University, Hunan Province 411105, China

[‡]Department of Chemistry and Nebraska Center for Materials and Nanoscience, University of Nebraska-Lincoln, Lincoln, Nebraska 68588, United States

[§]Institute of Nano Science, Nanjing University of Aeronautics and Astronautics, Nanjing 210016, China

Supporting Information

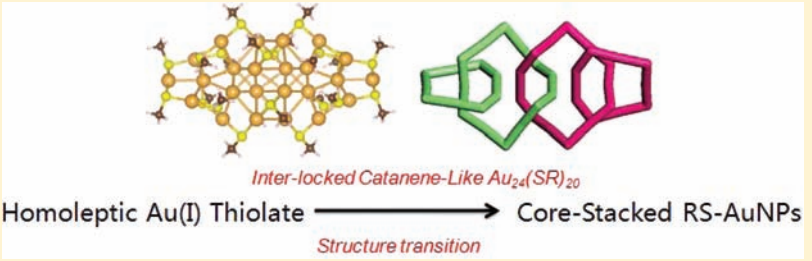

ABSTRACT: Atomic structure of a recently synthesized ligand-covered cluster $Au_{24}(SR)_{20}$ [*J. Phys. Chem. Lett.*, **2010**, *1*, 1003] is resolved based on the developed classical force-field based divide-and-protect approach. The computed UV−vis absorption spectrum and powder X-ray diffraction (XRD) curve for the lowest-energy isomer are in good agreement with experimental measurements. Unique catenane-like staple motifs are predicted for the first time in core-stacked thiolate-group (RS−) covered gold nanoparticles (RS−AuNPs), suggesting the onset of structural transformation in RS−AuNPs at relatively low Au/SR ratio. Since the lowest-energy structure of $Au_{24}(SR)_{20}$ entails interlocked $Au_5(SR)_4$ and $Au_7(SR)_6$ oligomers, it supports a recently proposed growth model of RS-AuNPs [*J. Phys. Chem. Lett.*, **2011**, *2*, 990], that is, $Au_n(SR)_{n-1}$ oligomers are formed during the initial growth of RS−AuNPs. By comparing the Au-core structure of $Au_{24}(SR)_{20}$ with other structurally resolved RS−AuNPs, we conclude that the tetrahedral Au_4 motif is a prevalent structural unit for small-sized RS−AuNPs with relatively low Au/SR ratio. The structural prediction of $Au_{24}(SR)_{20}$ offers additional insights into the structural evolution of thiolated gold clusters from homoleptic gold(I) thiolate to core-stacked RS−AuNPs. Specifically, with the increase of interfacial bond length of Au(core)−S in RS−AuNPs, increasingly larger "metallic" Au-core is formed, which results in smaller HOMO−LUMO (or optical) gap. Calculations of electronic structures and UV−vis absorption spectra of $Au_{24}(SR)_{20}$ and larger RS−AuNPs (up to ∼2 nm in size) show that the ligand layer can strongly affect optical absorption behavior of RS−AuNPs.

1. INTRODUCTION

Synthesis and characterization of thiolate group covered gold nanoparticle (RS−AuNP) have attracted increasing attention over the past few years due to their unique physicochemical properties and promising applications in catalysis, nanotechnology, and chemical biology.[1−6] Numerous experimental and theoretical studies have been devoted to the synthesis or characterization of RS−AuNPs in the size range of 1−2 nm.[7−13] Although most RS−AuNPs exhibit distinct UV−vis absorption spectra, electrochemical properties, and catalytic properties, determination of their atomic structure is still a challenging task largely because single crystals of most RS−AuNPs are difficult to make.

The first major breakthrough in total structure determination of RS−AuNP was achieved by Jadzinsky et al. who attained single crystals of $Au_{102}(p\text{-MBA})_{44}$ (where *p*MBA is *para*-mercapto benzoic acid, $SC_7O_2H_5$).[14] Later, atomic structure of the second RS−AuNP $Au_{25}(SCH_2CH_2Ph)_{18}^-$ was determined by several groups independently through experimental[15a,b] and theoretical studies.[16] These studies reveal that the Au cores inside $Au_{102}(p\text{-MBA})_{44}$ and $Au_{25}(SCH_2CH_2Ph)_{18}^-$ clusters are highly symmetric (with quasi-D_{5h} and quasi-I_h point group symmetry, respectively) and are fully covered by a number of staple motifs with different lengths, including −RS−Au−RS− and −RS−Au−RS−Au−RS−. Insights obtained from the determination of atomic structure of $Au_{102}(p\text{-MBA})_{44}$ and $Au_{25}(SCH_2CH_2Ph)_{18}^-$ have inspired great interests in exploration of more generic structural evolution rule and the origin of high stability of certain RS−AuNPs with specific composition.

Received: September 10, 2011
Published: January 15, 2012

dx.doi.org/10.1021/ja208559y | *J. Am. Chem.Soc.* 2012, 134, 3015−3024

Over the past few years, a number of RS−AuNPs such as $Au_{19}(SR)_{13}$,[9i] $Au_{20}(SR)_{16}$,[9b] $Au_{38}(SR)_{24}$,[9g] $Au_{40}(SR)_{24}$,[9f] $Au_{44}(SR)_{28}^{2-}$,[1f] $Au_{68}(SR)_{34}$,[8] and $Au_{144}(SR)_{60}$[9a] have been isolated and characterized by the mass spectrometry (MS), powder XRD, electrochemical, and optical absorption measurements. However, the lack of atomic structures for most of these clusters hinders our understanding of their structure−function relationship. Considerable theoretical efforts have also been devoted to predicting atomic structures of RS−AuNPs. Several structural models have been proposed for $Au_{12}(SR)_9^+$,[17a] $Au_{19}(SR)_{13}$,[17b] $Au_{20}(SR)_{16}$,[18,19] $Au_{38}(SR)_{24}$,[20−23] $Au_{44}(SR)_{28}^{2-}$,[24] and $Au_{144}(SR)_{60}$[25] via density functional theory (DFT) calculations (summarized in Table 1). For example, two improved theoretical models of $Au_{38}(SR)_{24}$[22,23] have been confirmed by a recent experiment with the single-crystal measurement.[9g] Also, for $Au_{20}(SR)_{16}$, the calculated UV−vis absorption spectrum based on a theoretically predicted structure appears to be in good agreement with the experimental data.[19] To understand high stability of certain magic number RS−AuNPs, Häkkinen et al. have proposed a superatom model[26] such that the total number of free valence electron (n^*) associated with an RS−AuNP can be counted using the formula $n^* = Nv_A - M - z$, where the Nv_A is the number of Au($6s^1$) electron associated with the Au core, and M and z are the number of electron-withdrawing ligands (staple motifs) and the net charge of cluster, respectively. Based on this model, one can calculate n^* of $Au_{25}(SR)_{18}^-$ and $Au_{102}(SR)_{44}$ to be 8e and 58e, respectively, which are indeed the magic electronic numbers that correspond to closed electron shells within the framework of spherical *jellium* model. In addition to the electronic interpretation, Reimers et al. and Han et al. performed a detailed thermodynamic analysis on the $Au_{102}(SR)_{44}$ cluster and gave additional explanation of high stability of $Au_{102}(SR)_{44}$.[27,28]

Despite many experimental and theoretical efforts, a question that remains unanswered is how the structural evolution of thiolated gold clusters from the polymer-like homoleptic Au(I) thiolates (with the same ratio of Au and −SR group) to core-stacked nanoparticles (Au atom excess to the −SR ligand) develops. The homoleptic Au(I) thiolate is a common reagent for synthesis of RS−AuNPs.[29] Previous experimental studies have shown that growth of RS−AuNPs was significantly affected by the reaction conditions, for example, type of solvent and amount of reducing agents, which are often utilized to control the synthesis of RS−AuNPs with specific composition.[1b,d,f,9a−i,29−33] One growth mechanism proposed previously is that RS−AuNPs can grow through a basic step of reduction of homoleptic Au(I) thiolates, in which the Au core is built upon excess Au atoms with valence between 0 and 1, and then stabilized by surrounding thiolates.[32,34] However, it remains an open question about detailed kinetic process during the Au core formation. Notably, recent mass spectrometry experiments have demonstrated irreversible conversion of $Au_{38}(SR)_{24}$, $Au_{68}(SR)_{34}$, and $Au_{102}(SR)_{44}$ to the smaller $Au_{25}(SR)_{18}$ cluster in a fresh sample of mixed RS−AuNPs,[8,35] which suggested a close structural relationship among Au cores in these seemingly very different clusters. By examining the core structure of $Au_{25}(SR)_{18}^-$, $Au_{38}(SR)_{24}$, and $Au_{102}(SR)_{44}$, Dass speculated that the 13 atom icosahedron, decahedron, and octahedron are common structural units (Scheme 1a and 1b).[8] Note that the 13 atom icosahedron, decahedron, and octahedron can be interconverted through rotation of triangle faces. However, previous theoretical studies predict an edge-fused bi-tetrahedron Au_8 core for $Au_{20}(SR)_{16}$ and a bipyramid Au_6 core for $Au_{12}(SR)_9^+$ (Scheme 1c), respectively.[17a,19] Note also that, an extended staple motif −RS−Au−RS−Au−RS−Au−RS− has also been observed for the first time in the $Au_{20}(SR)_{16}$.[19] These results suggest that when the Au/SR ratio approaches 1:1 (marked as the transition region from homoleptic Au(I) thiolate to core-stacked RS−AuNPs; see below), the Au core and staple motifs may undergo major structural changes. A better understanding of the structural transition in Au cores and staple motifs from the polymer-like homoleptic Au(I) thiolate to core-stacked RS−AuNPs is important to the establishment of growth mechanism of RS−AuNPs.

Besides mass spectrometry, optical absorption properties of RS−AuNPs can be strongly affected by the size and composition of the clusters. Table 1 summarizes optical absorption property of known thiolated gold clusters reported in the literature. It can be seen that the optical absorption edge of RS−AuNPs does not show obvious relationship with their size or with their Au/SR ratio. However, a rapid decrease of the highest occupied molecular orbital−lowest unoccupied molecular orbital (HOMO−LUMO)

Table 1. Comprehensive Summary of Properties of Various Thiolated Gold Clusters Reported in the Literature[a]

			type and number of staple motifs						
RS−AuNPs	N_{Au}/N_S	Au core	−SR−Au−SR−Au−SR−	−SR−Au−SR−Au−SR−	−SR−Au−SR−Au−SR−Au−SR−	−SR−Au−SR−Au−SR−Au−SR−Au−SR−	−SR−Au−SR−Au−SR−Au−SR−Au−SR−Au−SR−	n^*	H−L gap (eV)
$Au_{10}(SR)_{10}$[37]	1.00	Au_2	0	0	0	2	0	0	2.70
$Au_{24}(SR)_{20}$[9c]	1.20	in this work							1.47
$Au_{20}(SR)_{16}$[19]	1.25	Au_8	(0	0	4	0	0)[b]	4	2.10
$Au_{12}(SR)_9^+$[17a]	1.33	Au_6	(0	3	0	0	0)[b]	2	1.70
$Au_{25}(SR)_{18}^-$[15,16]	1.39	Au_{13}	0	6	0	0	0	8	1.33
$Au_{19}(SR)_{13}$[17b]	1.46	Au_{11}	(2	3	0	0	0)[b]	6	1.50
$Au_{44}(SR)_{28}$[2-1f,23]	1.57	Au_{24}	(4	8	0	0	0)[b]	18	1.60
$Au_{38}(SR)_{24}$[21,22,25]	1.58	Au_{23}	3	6	0	0	0	14	0.90
$Au_{40}(SR)_{24}$[9f]	1.67	unknown						16	1.00
$Au_{68}(SR)_{34}$[8a]	2.00	unknown						34	1.20
$Au_{102}(SR)_{44}$[14,36]	2.32	Au_{79}	19	2	0	0	0	58	0.50
$Au_{144}(SR)_{60}$[9,24]	2.40	Au_{114}	(30	0	0	0	0)[b]	84	0

[a] n^* represents the number of free metal valence electrons. H−L gap refers to the energy gap between the highest occupied (HOMO) and lowest unoccupied molecular orbitals (LUMO). [b] The staple motif combinations shown in the parentheses are theoretically predicted and therefore must await future experimental validation.

Scheme 1. Schematic Illustration of Basic Structural Motifs of Au Cores in Representative RS−AuNPs

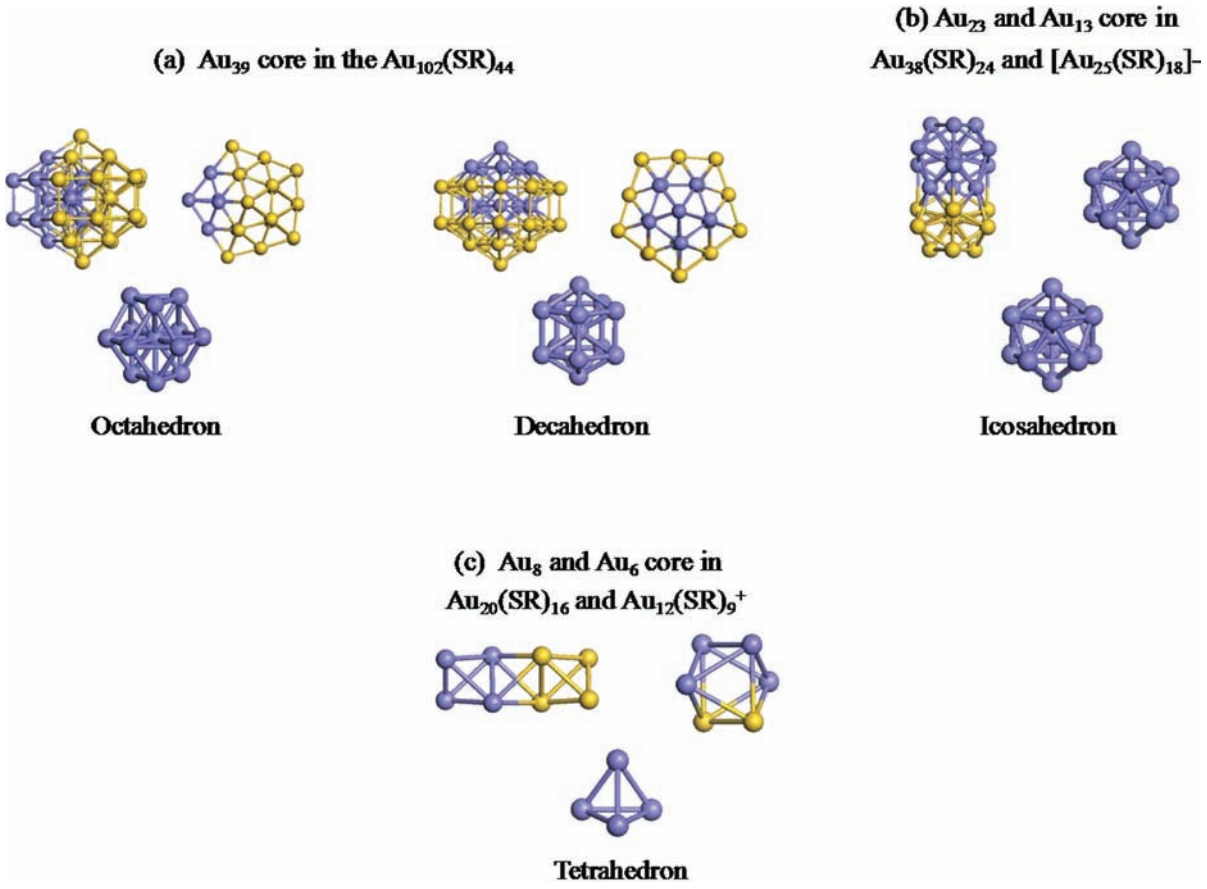

gap can be seen with the increase of the cluster size. For example, the largest optical absorption gap of 2.10 eV is found for $Au_{20}(SR)_{16}$,[9a,19] and a ∼0.5 eV gap for the $Au_{102}(SR)_{44}$ has been computed[36] and measured recently in experiments.[14b] As for the larger (>2 nm) cluster $Au_{144}(SR)_{60}$, both experimental measurements and theoretical calculations suggest zero HOMO−LUMO gap.[9a,25] The superatom model illustrates the closed-shell electronic structure of $Au_{25}(SR)_{18}^-$ and $Au_{102}(SR)_{44}$,[26] which successfully explains their sizable HOMO−LUMO gap. However, the superatom concept cannot fully explain the evolution trend of HOMO−LUMO gap for larger and larger RS−AuNPs. Especially, for the RS−AuNPs with relatively low Au/SR ratio and small Au core, such as $Au_{12}(SR)_9^+$,[17a] $Au_{20}(SR)_{16}$,[19] and $Au_{24}(SR)_{20}$,[9c] which show large variation of the HOMO−LUMO gap with structural composition. A recent theoretical study on the $Au_{38}(SR)_{24}$ indicates that the chiral structure of the ligand layer contributes to the strong circular dichroism (CD) spectrum in the excitations below 2.2 eV, suggesting a strong effect of interfacial structure of ligand layer on optical absorption properties of RS−AuNPs.[23] Hence, it is important to explore effects of ligand layer on the UV−vis absorption spectra of RS−-AuNPs.

In this article, we aim to address two key issues: (1) structural transition of RS−AuNPs from the homoleptic Au(I) thiolate to the core-stacked particle; and (2) the effect of ligand layer structures on the optical absorption spectra of RS−AuNPs in the transition region from the Au(I) thiolate to the core-stacked nanoparticles. Both issues are examined based on the predicted atomic structure of a recently synthesized RS−AuNP, that is, $Au_{24}(SR)_{20}$.[9c] The $Au_{24}(SR)_{20}$ is of special interest due to its small Au/S ratio (1.2), ideally a benchmark model for understanding the structural transition of RS−AuNPs from the homoleptic Au(I) thiolate to the core-stacked RS−AuNPs. To determine the cluster structure, a combined classical force field and basin-hopping search has been tested, which turns out to be an efficient way to generate sensible Au core structures. In addition, time-dependent density-functional theory (TD-DFT) calculations are carried out for a series of thiolated gold clusters, from the homoleptic Au(I) thiolate to core-stacked RS−AuNPs, to investigate atomic orbital contribution to the transition molecular orbitals that are relevant to the UV−vis absorption spectra. In particular, the UV−vis absorption spectrum of $Au_{102}(SCH_3)_{44}$ is computed, which offers additional insight into the electronic structure of RS−AuNPs with size up to 2 nm.

2. COMPUTATIONAL METHODS

2.1. Structure Prediction of RS−AuNP: A Force-Field Based Divide-and-Protect Approach. Global searches of potential energy surfaces of RS−AuNPs are computationally very demanding by using global optimization methods such as the genetic algorithm (GA),[38,39] simulation annealing (SA),[40] and basin-hopping (BH),[41] due largely to RS−AuNPs' complex atomic structures. Hence, for predicting the structure of the $Au_{24}(SR)_{20}$ cluster, we follow the divide-and-protect idea originally proposed by Häkkinen et al.,[21] that is, a $Au_m(SR)_n$ cluster can be viewed as an Au_N core fully covered by various staple motifs (with known structures but different lengths). As such, we have previously proposed an expanded structural formula[19,22] for $Au_m(SR)_n$, that is, $Au_{a+a'}[Au(SR)_2]_b[Au_2(SR)_3]_c[Au_3(SR)_4]_d...$, where $Au_{a+a'}$ represents the Au core, and *b*, *c*, and *d* denote the number of level-1, -2, and -3 staple motifs with increasing length (Scheme 2). It is worth noting that the type of staple motifs selected in the formation of clusters depends strongly on the ratio of Au/SR in the RS−AuNP (see Results and Discussion below). Since structures of staple motifs

dx.doi.org/10.1021/ja208559y | J. Am. Chem.Soc. 2012, 134, 3015−3024

Scheme 2. Illustration of the Force-Field Based Divide-and-Protect Approach

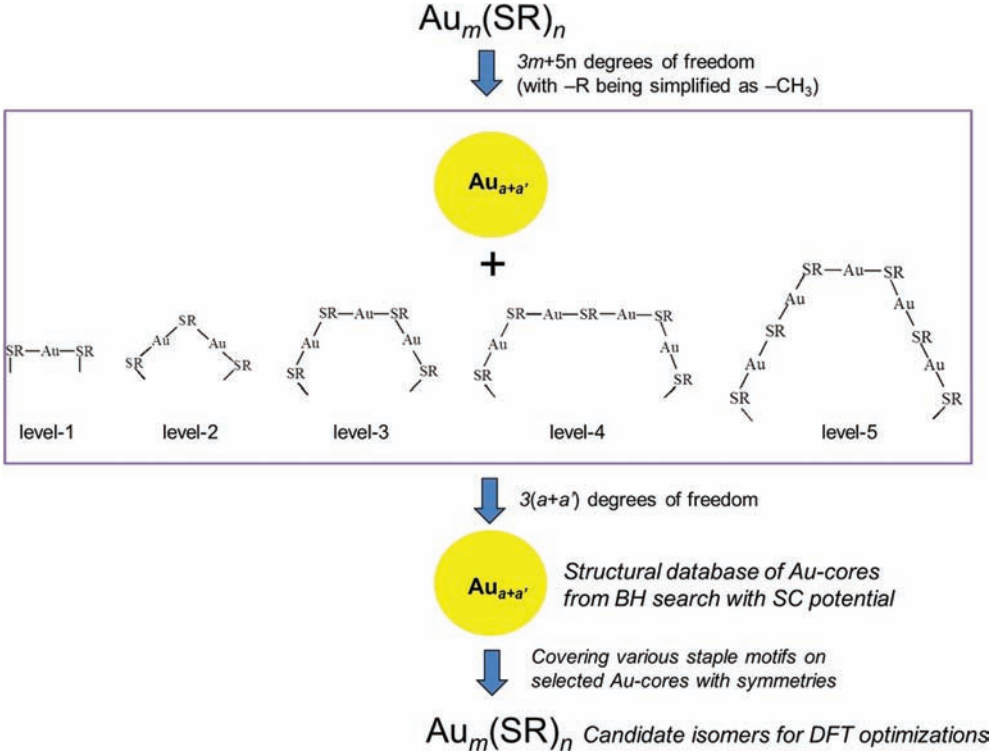

are already known, the structural prediction of RS–AuNPs can be initially focused on the search of proper Au core structure ($Au_{a+a'}$, shown in Scheme 2). As such, the degrees of freedom for each cluster are reduced from $3m + 5n$ (with $R = CH_3$) to $3(a + a')$, for which the computational cost is dramatically reduced. Hence, the search of structure of RS–AuNPs can be converted to the search of a proper Au core structure with staple motifs flawlessly covered.

The important question is how to find a sensible Au core structure. First, constraint conditions for all the structures should be considered,[19,21,22] for example, each terminal S atom of a staple motif can bind with only one Au atom belonging to the Au core (so that $a' = 2b + 2c + 2d$). Under this constraint, the number of conceivable structural candidates for the Au core is further reduced. We have developed a simple classical force-field approach to generate a database of Au cores and to quickly determine possible Au core structures. The force field parameters for Au are the Sutton–Chen potential.[42] Note that the use of the BH algorithm in this case is no longer to find out the global minimum of the Au core, rather to generate a structural database for the Au core. From this database, we can select several highly reasonable structures, typically possessing relatively high point group symmetry. Indeed, several experimental and theoretical studies of structure of thiolate protected gold clusters have indicated the cover of ligand may significantly shape the structure of the Au cluster.[15–26,43,44] The Au atoms in the protected core tend to form symmetric structures, as the result of the nominally charged Au core caused by ligand protection. In comparison to the DFT computations, the Sutton–Chen potential favors the geometric packing of gold atoms. Therefore, the use of the Sutton–Chen potential is in advantage of a quick search of high symmetric core structures. Once the target Au cluster (e.g., Au_N, $N = a + a'$) has the symmetric structure and satisfies the constrain condition described above, the cluster is chosen as a candidate core structure covered with staple motifs. A DFT optimization is then applied to generate a local minimum structure of assembled $Au_m(SR)_n$, as described in Scheme 2.

The force-field based divide-and-protect approach has been validated with three benchmark RS–AuNPs, that is, $Au_{25}(SR)_{18}^-$, $Au_{38}(SR)_{24}$, and $Au_{102}(SR)_{44}$. The predicted three Au core structures all possess high symmetry, namely, I_h-Au_{13}, D_{3h}-Au_{23}, and D_{5h}-Au_{79}, which are all stable minima based on the Sutton–Chen (SC) potential, suggesting the structural search of the three Au clusters (Au_{13}, Au_{23}, and Au_{79}) can yield realistic Au core structures for the three known RS–AuNPs. However, we find that the DFT-based global search is not effective for generating a Au core database, not only because of the high computational cost, but also several high-symmetry Au core structures such as the bi-icosahedra D_{3h}-Au_{23} structure is not a local minimum in the DFT potential energy surface and hence would be missed in the global search. A schematic illustration of construction of the starting geometry of an isomer of $Au_{24}(SR)_{20}$ based on the force-field based divide-and-protect method is displayed in the Supporting Information (Scheme S1).

2.2. Geometrical Optimizations, Powder XRD, and TD-DFT Calculations. DFT optimizations of the $Au_{24}(SR)_{20}$ isomers are performed using DMol^3 4.3,[45] Amsterdam Density Functional (ADF 2010),[46] and Gaussian09[47] software packages, all within the generalized gradient approximation with the Perdew–Burke–Ernzerhof (PBE) functional.[48] With the DMol^3 package, the *d*-polarization included basis set (DND) is used for C, H, S elements, while the effective core potential (ECP) approximation with partial accounts of scalar relativity is used for the Au element. For the 10 lowest-lying structures obtained from DMol^3 PBE/DND calculations, we reoptimize their structures using the triple-ζ polarized (TZP) basis set with inclusion of scalar relativistic effect via zeroth-order regular approximation (ZORA) implemented in the ADF package. The spin–orbit coupling effects on the relative stability of the three lowest-lying isomers are also examined at the PBE/TZP level. Lastly, the three lowest-lying structures from ADF PBE/TZP calculations are further examined using the meta-hybrid GGA functional TPSSh[49] and M06,[50] and Møller–Plesset second-order perturbation (MP2)[51] theory with the basis sets LANL2DZ for Au and 6-31G(d) for C, H, and S atoms, respectively. The performance of various DFT functional such as PBE, TPSSh, and M06 on the prediction of relative stabilities of gas-phase gold clusters has been discussed previously.[52] The two-dimensional (2D) to three-dimensional (3D) transition region of small sized gold clusters is correctly predicted by the TPSSh and M06 functional as observed by experiments.

dx.doi.org/10.1021/ja208559y | J. Am. Chem.Soc. 2012, 134, 3015–3024

The theoretical powder X-ray diffraction (XRD) curve is calculated using the Debye formula:

$$I(s) = \sum_i \sum_{j \neq i} \frac{\cos\theta}{(1 + \alpha\cos(2\theta))} \exp\left(-\frac{Bs^2}{2}\right) f_i f_j \frac{\sin(2\pi d_{ij})}{2\pi d_{ij}}$$

where s is the diffraction vector length and θ is the scattering angle, satisfying $s = 2\sin\theta/\lambda$. The λ and α are determined by the experimental setup and are set to be 0.1051967 nm and 1.01, respectively. B is the damping factor, which reflects thermal vibrations, and is set to be 0.03 nm^2. The corresponding atomic numbers are used for the scattering factors f_i. d_{ij} is the distance between atoms i and j. The atomic distance d_{ij} used in the calculation is taken from the optimized structure of clusters based on TPSSh/LANL2DZ (for the Au atom) and 6-31G(d) (for C, H, S atoms). Using $Au_{25}(SH)_{18}^-$ as a model system, the computed averaged Au−Au distance from the central Au atom to the shell Au atom is 2.804 Å, close to the experimental value 2.782 Å in the crystal structure of $Au_{25}(SCH_2CH_2Ph)_{18}^-$.[15]

The TD-DFT computation of optical absorption spectra and circular dichroism (CD) spectra is performed at the PBE/TZP level of theory, using the ADF program package. The TD-DFT calculations evaluates lowest 200 singlet-to-singlet excitation energies for $Au_{24}(SR)_{20}$. Rotatory strengths are computed using the RESPONSE module in ADF. The computed rotatory strengths R are in units of esu^2 cm^2.

3. RESULTS AND DISCUSSION

3.1. Structure Prediction of $Au_{24}(SR)_{20}$: A Prolate Au_8 Core with Catenane-Like Staple Motifs. For $Au_{24}(SR)_{20}$, its Au/S ratio is slightly less than that of $Au_{20}(SR)_{16}$, which possesses a novel level-3 staple motif as predicted due to its relatively small Au/SR ratio (cf. Table 1).[19] The smaller Au/SR ratio in the $Au_{24}(SR)_{20}$ implies that longer (higher-level) staple motifs may exist in light of a general rule that the number of longer (or higher-level) staple motifs increases with decreasing the Au/S ratio.[19,53] On the basis of the core/staple motif division scheme given above, we consider all possible combinations of the Au core and staple motifs with different lengths for $Au_{24}(SR)_{20}$ (c.f. Table S1 in the Supporting Information), including even the level-4 and level-5 staple motifs because of the smaller Au/SR ratio. Specifically, the structural division of $Au_{24}(SR)_{20}$ is written as $Au_{a+a'}[Au(SR)_2]_b[Au_2(SR)_3]_c[Au_3(SR)_4]_d[Au_4(SR)_5]_e[Au_5(SR)_6]_f$ where positive integers a, a', b, c, d, e, and f satisfy $a + a' + b + 2c + 3d + 4e + 5f = 24$ and $2b + 3c + 4d + 5e + 6f = 20$, respectively. Another constraint is that each of surface Au atoms (a') in the Au core is bonded with one terminal S atom of a staple motif so that $a' = 2(b + c + d + e + f)$. With this structural constraint condition, only five distinctive structural divisions are allowed, namely, $Au_8[Au_3(SR)_4]_2[Au_5(SR)_6]_2$, $Au_8[Au_3(SR)_4][Au_4(SR)_5]_2[Au_5(SR)_6]$, $Au_8[Au_4(SR)_5]_4$, $Au_8[Au(SR)_2][Au_5(SR)_6]_3$, and $Au_8[Au_2(SR)_3][Au_4(SR)_5][Au_5(SR)_6]_2$, which all contain a Au_8 core. Next, a number of Au_8 core structures are generated via the BH search based on the SC potential for Au_8. From the generated Au_8 core database, a few symmetric structures are selected, followed by a full coverage of these Au_8 cores by proper number of staple motifs based on the five structural divisions. There are 52 isomers collected for the subsequent DFT optimizations, for which the −R group is simplified as a methyl ($-CH_3$) group to reduce computing cost. The 10 lowest-lying isomers obtained at the PBE/DND level are reoptimized at the PBE/TZP level. Calculated relative energies and structures of seven isomers with higher energies are given in Figure S1 of the Supporting Information.

Figure 1 shows optimized structures of three lowest-lying isomers of $Au_{24}(SR)_{20}$ (**Iso1**−**Iso3**). Relative energies of the three isomers at different levels of theory are shown in Table 2.

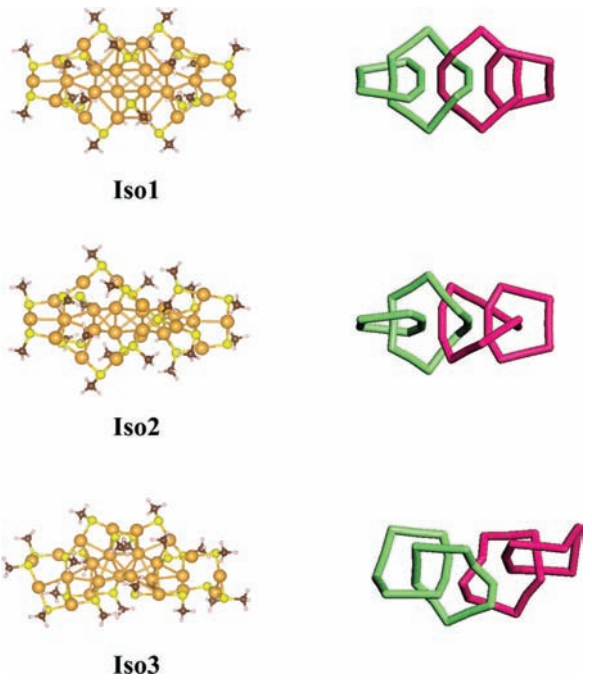

Figure 1. Optimized structures of three lowest-lying isomers **Iso1**−**Iso3** (left panel). The methyl groups are removed for clarity in the topological structural model (right panel). The Au, S, C, and H atoms are in khaki, yellow, gray, and white colors, respectively (left panel). Another atomic view of interlocked topological structural model is given in the Supporting Information with detailed Cartesian coordinates (the final section of SI).

Table 2. Relative Energies (eV) of Iso1−Iso3 at Three Levels of Theory

isomers	PBE/TZP with inclusion of spin−orbit coupling	TPSSh/LANL2DZ and 6-31G(d)	M06/LANL2DZ and 6-31G(d)	MP2/LANL2DZ and 6-31G(d)[a]
Iso1	0.00	0.00	0.00	0.00
Iso2	0.07	0.24	0.20	1.15
Iso3	0.15	0.34	0.49	1.22

[a]The MP2 single energy is calculated based on the optimized geometries of TPSSh/LANL2DZ and 6-31G(d).

The PBE/TZP with inclusion of the spin−orbit coupling, the TPSSh and M06/LANL2DZ (for Au)/6-31G(d) (for S, C, H), and MP2/LANL2DZ (for Au)/6-31G(d) (for S, C, H) single-point energy calculation at TPSSh optimized geometries all indicate that **Iso1** has the lowest energy. As shown in Figure 1, **Iso1** has a structural division of $Au_8[Au_3(SR)_4]_2[Au_5(SR)_6]_2$, with a prolate Au_8 core (with near-D_{2d} point group symmetry) and interlocked $[Au_3(SR)_4]$ and $[Au_5(SR)_6]$ staple motifs. The entire structure of **Iso1** exhibits D_2 symmetry (at the tolerance of 0.1 Å). In **Iso1**, four terminal S atoms in two level-3 $[Au_3(SR)_4]$ motifs are bonded with two Au dimers on the opposite sides of the Au_8 core. The remaining four Au core atoms are bonded with the four terminal S atoms of two level-5 $[Au_5(SR)_6]$ motifs.

The most interesting feature of **Iso1** is the presence of two level-3 $[Au_3(SR)_4]$ and two level-5 $[Au_5(SR)_6]$ motifs, interlocked like a linked chain, from one end to another of the prolate Au_8 core. Hereafter, we name these motifs catenane-like staple motifs. To our knowledge, such catenane-like staple motifs

dx.doi.org/10.1021/ja208559y | J. Am. Chem.Soc. 2012, 134, 3015−3024

have not been previously observed in core-stacked RS−AuNPs but only found in Au(I) thiolate catenane $Au_{10}(SR)_{10}$ and $Au_{12}(SR)_{12}$ via both experiment[37] and theory.[54] Topologically, **Iso1** can be also viewed as a combination of two sets of symmetric interlocked oligomers $Au_5(SR)_4$ and $Au_7(SR)_6$. In fact, a recently proposed growth mechanism of RS−AuNPs indicates that $Au_n(SR)_{n-1}$ oligomers are likely formed during the initial growth of RS−AuNPs from the reduction of homoleptic Au(I) thiolates.[34] The appearance of interlocked structure in **Iso1** supports this proposed mechanism. On the other hand, the orientation of staple motifs may affect relative stability of thiolated gold clusters.[23] Here, the second lowest-lying structure (**Iso2**) has the same Au_8 core as **Iso1** but a different orientation for two level 5 staple motifs (cf. Figure 1). The change in orientations of staple motifs results in 0.24 eV (TPSSh result) higher in energy compared to **Iso1**. The third lowest-lying isomer **Iso3** has a structural division of $Au_8[Au_3(SR)_4]_4$, in which, a distorted Au_8 core with near-C_2 symmetry is covered by two sets of identical catenane-like $[Au_4(SR)_5][Au_4(SR)_5]$ staple motifs. Calculations at other levels of theory also confirm that **Iso3** is less stable than **Iso1** and **Iso2** (cf. Table 2).

To our knowledge, the level-5 and catenane-like staple motifs are predicted for the first time in the RS−AuNPs. The appearance of such highly extended and interlocked staple motifs in $Au_{24}(SR)_{20}$ is due largely to the small Au/SR ratio. In $Au_{20}(SR)_{16}$, four level-3 $[Au_3(SR)_4]$ staple motifs are predicted to cover the Au_8 core without interlocking.[19] In fact, the energy computation indicates that isomers of $Au_{24}(SR)_{20}$ with catenane-like staple motifs all have much lower energy than those without interlocked staple motifs (cf. the Supporting Information, Figure S1), suggesting that the interlocking arrangement of staple motifs is energetically more favorable for RS−AuNPs with low Au/S ratios. In addition, the prolate shape of the Au_8 core in $Au_{24}(SR)_{20}$ satisfies the superatom description of RS−AuNPs. According to the electron counting rule of the superatom model,[26] the $Au_{24}(SR)_{20}$ has four free metal valence electrons (4*e*), suggesting a prolate core structure according to the Clemenger−Nillson model,[55] similar to that previously found in $Au_{20}(SR)_{16}$.[19]

3.2. Comparisons with Experimental Measurements.

To further support that **Iso1** is the best candidate structure for $Au_{24}(SR)_{20}$, UV−vis absorption spectrum and powder X-ray diffraction (XRD) curves are computed for the 10 lowest-lying isomers (**Iso1**−**Iso10** as shown in the Supporting Information, Figure S1). In Figure 2, computed UV−vis absorption spectra of **Iso1**−**Iso3** are compared with the original experimental absorption spectrum. It can be seen that the optical band-edges of **Iso1**−**Iso3** are 1.47, 1.47, and 1.31 eV, respectively. The first two are in excellent agreement with the measured band-edge of 1.47 eV. Indeed, the PBE functional has been found to reasonably reproduce the optical-edge of most structure known thiolated gold clusters.[14b,15b,16,22,23,36,56]

In the experimental UV−vis absorption curve, a feature absorption peak locating around 1.6 eV is clearly found, which is predicted from the TD-DFT excitation energy curve of both **Iso1** and **Iso2**. Above 1.8 eV, the experimental curve does not exhibit obvious feature absorption peaks. A broad absorption band (***b***) locating nearly between 1.7 and 2.6 eV with gradually increased absorption strength is found. The theoretical excitation-energy curve of **Iso1** shows the best agreement with the experimental absorption band in this energy region. Moreover, the excitation-energy curve of **Iso1** shows pronounced oscillator strength around 3.1 eV (peak ***c***), which

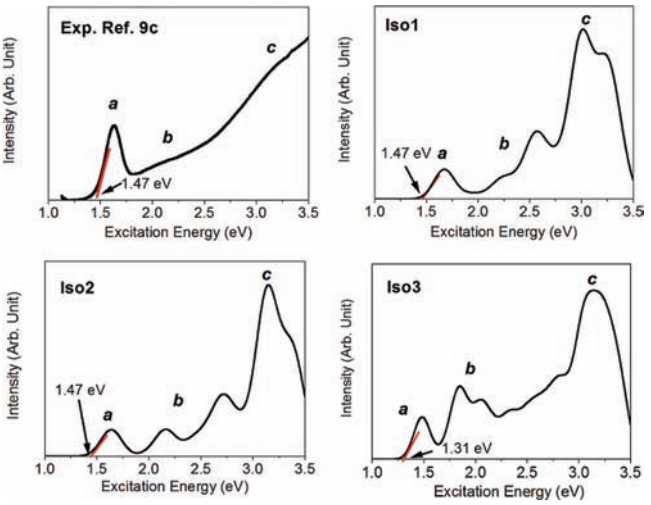

Figure 2. Comparison of the experimental (upper left panel) and theoretical UV−vis absorption spectra of $Au_{24}(SR)_{20}$. In theoretical calculations, the −R group is simplified as $-CH_3$. The red lines define the optical band edge. The experimental curve is taken from ref 9c.

is in good agreement with the experimental curve. Indeed, the strong absorption at ∼3 eV is a common feature absorption peak of thiolate protected gold clusters, which has been featured in several RS−AuNPs, such as $Au_{12}(SR)_9^+$,[17a] $Au_{20}(SR)_{16}$,[18,19] $Au_{25}(SR)_{18}^-$,[15,16,56] and $Au_{38}(SR)_{24}$.[22,23] Additional investigation of effects of orientations of methyl groups in **Iso1** on the relative stabilities and shape of excitation energy curve is performed (Figure S2 in the Supporting Information). It is found that the orientation of methyl groups affects slightly the relative stability of the cluster and the shape of the excitation energy curve. Moreover, the UV−vis absorption curve of **Iso1** is also computed based on different starting models optimized by LDA-Xα/TZP, KT2/TZP[46] and TPSSh/LANL2DZ and 6-31G(d) as shown in Figure 3. It is worth noting that weak aurophilic interactions are prevalent in the predicted structure of $Au_{24}(SR)_{20}$ among Au atoms in different staple motifs. It is known that the GGA functional tends to underestimate the strength of weak interactions. In present, the LDA-Xα/TZP optimization yields shorter Au(I)−Au(I) atomic distances than that obtained from PBE/TZP for the **Iso1**, which eventually leads to smaller optical absorption gap (1.38 eV) and increased oscillator strength of absorption band ***b*** as shown in Figure 3. The excitation energy curve obtained based on KT2/TZP and TPSSh/TZP geometries is similar to that based on PBE/TZP geometry.

Additionally, the simulated XRD curves of **Iso1**−**Iso3** (based on TPSSh optimized geometries) are compared with the experimental XRD curve in Figure 4. Overall, **Iso1** shows the best agreement with the experimental curve. For **Iso2** and **Iso3**, their second and third peaks are slightly shifted compared to the corresponding experimental peaks. On the basis of computed relative energies, optical absorption curves, and XRD curves for **Iso1**−**Iso3**, we conclude the **Iso1** with two sets of interlocked $Au_5(SR)_4$ and $Au_7(SR)_6$ oligomers is the best candidate for the structure of $Au_{24}(SR)_{20}$.

Recent experimental and theoretical studies of $Au_{38}(SR)_{24}$ demonstrate that different arrangement of staple motifs can strongly affect their circular dichroism (CD) spectra.[23] In present, the S_4 symmetry of **Iso2** indicates it should not exhibit a CD signal, but **Iso1** and **Iso3** with D_2 and C_1 symmetries will

dx.doi.org/10.1021/ja208559y | J. Am. Chem.Soc. 2012, 134, 3015−3024

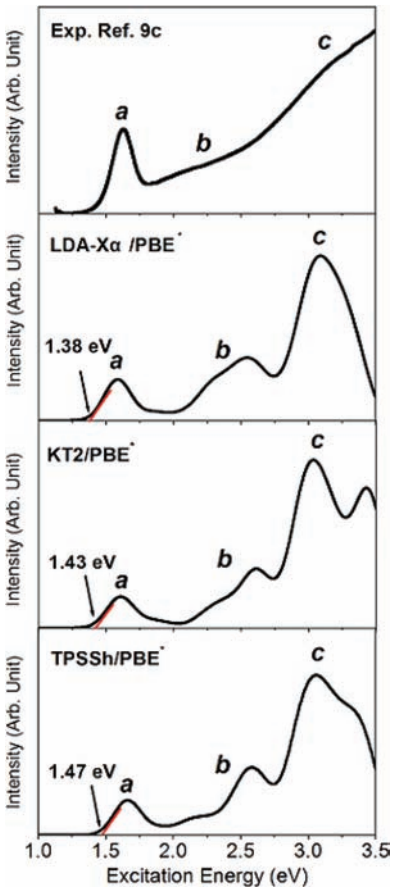

Figure 3. Comparison of the experimental and theoretical UV−vis absorption spectra of **Iso1** based on different geometries. *The geometric structure of **Iso1** is reoptimized based on LDA-Xα/TZP, KT2/TZP and TPSSh/LANL2DZ + 6-31G(d) level of theory, respectively; the excitation energy is computed using PBE functional. The red lines define the optical band edge. The experimental curve is taken from ref 9c.

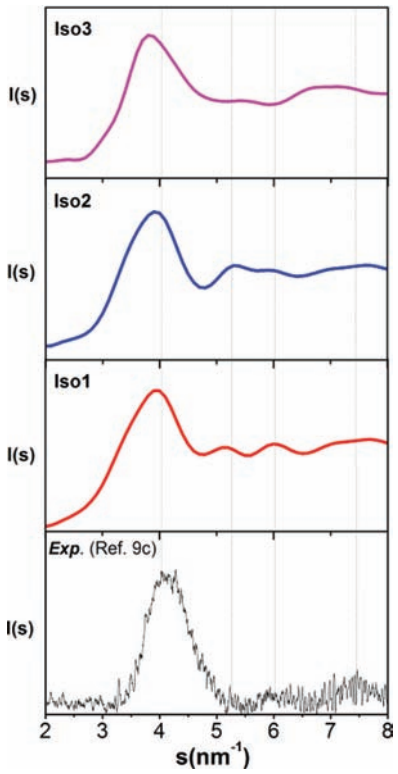

Figure 4. Comparison of the experimental XRD curve with simulated XRD curves of **Iso1**−**Iso3**.

exhibit CD signals to some extent. The CD spectra of **Iso1**−**Iso3** are thus computed (at the PBE/TZP level) and are shown in the Supporting Information, Figure S3. The differences in CD signals among three isomers can be clearly seen. **Iso1** exhibits pronounced rotator strength, due to the chiral distribution of staple motifs. In the CD spectrum of **Iso1**, the first and second major positive peaks, contributed mainly by the transition between orbitals of Au and S atoms in the staple motifs and Au core, suggest that the chiral arrangement of staple motifs can significantly enhance the rotatory strengths of excitations. In fact, **Iso1** has a higher symmetry (D_2) than **Iso3** (C_1 symmetry), in agreement with previous studies of $Au_{38}(SR)_{24}$[22] and phosphine-stabilized Au_{11}[57] clusters. For systems with higher chiral symmetry, the more intense CD signal is apparent compared those with lower symmetry.

3.3. Structural Evolution of RS−AuNPs from Homoleptic Au(I)−Thiolate to Core-Stacked Nanoparticles. The predicted **Iso1** structure of $Au_{24}(SR)_{20}$ offers additional insights into possible structural transitions in thiolated gold clusters from homoleptic Au(I) thiolate to core-stacked RS−AuNPs. In contrast to previously known structures of RS−AuNPs, the catenane-like staple motifs are only found in the homoleptic Au(I) thiolates that can exhibit either catenane, helix, or crown configuration.[37,54] The finding of catenane-like staple motifs in $Au_{24}(SR)_{20}$ suggests that, at low Au/SR ratio limit (i.e., approaching to 1:1), the interlocked staple motifs may become a prevalent conformation in RS−AuNPs. Moreover, both **Iso1** and **Iso2** of $Au_{24}(SR)_{20}$ have similar Au_8 cores as that of $Au_{20}(SR)_{16}$ (with Au/SR ratio = 1.25), which consists of two tetrahedral Au_4 units. Note that the tetrahedral Au_4 core has been predicted theoretically and observed experimentally for small nanoparticles such as $Au_{10}(SR)_8$[18] (with Au/SR ratio = 1.25) and $Au_4(PPh_3)_4^{2+}$.[58] Note also that a bipyramidal Au_6 core has been predicted for the $Au_{12}(SR)_9^+$ (with Au/SR ratio = 1.33)[17a] and observed previously in $Au_6(PPh_3)_6^{2+}$.[59] This bipyramidal Au_6 core can be viewed as edge-fusion of two Au_4 units (cf. Scheme 1c). These results suggest that a major structural transition for the Au core may occur when the Au/SR ratio approaches to a 1:1 limit. Recent MS experiments on $Au_{25}(SR)_{18}$ (with Au/SR ratio = 1.39), $Au_{38}(SR)_{24}$ (with Au/SR ratio = 1.58), $Au_{68}(SR)_{34}$ (with Au/SR ratio = 2.0), and $Au_{102}(SR)_{44}$ (with Au/SR ratio = 2.32) suggest that the 13-atom icosahedron, octahedron, and decahedron are basic structural unit for the inner Au cores (cf. Scheme 1).[8a,35] Hence, the close-packing tetrahedron Au_4 is concluded to be a common core unit for small-sized RS−AuNPs with relatively small Au/SR ratio (e.g., < 1.39 in this study). It is also worth noting that even lower Au/SR ratios have been found in some clusters such as $Au_{15}(SR)_{13}$ and $Au_{13}(SR)_{11}$.[60,61] It will be interesting to explore structures of latter clusters using the divide-and-protect procedure.

3.4. Electronic Structures of RS−AuNPs from Homoleptic Au(I)−Thiolate to Core-Stacked Nanoparticles. Electronic properties of RS−AuNPs can be partially manifested in their UV−vis absorption spectra. The superatom model has successfully explained why certain ligand-covered gold clusters, for example, $Au_{102}(SR)_{44}$ and $Au_{25}(SR)_{18}^-$, are highly

dx.doi.org/10.1021/ja208559y | J. Am. Chem.Soc. 2012, 134, 3015−3024

stable clusters.[26] However, the relationship between ligand layer structure and HOMO−LUMO gap of RS−AuNPs cannot be fully explained by the superatom model. As shown in the Supporting Information, Table S1, the HOMO−LUMO gaps of RS−AuNPs decrease rapidly from $Au_{25}(SR)_{18}^-$ to $Au_{102}(SR)_{44}$, which may be due to the formation of larger and larger metallic Au core in the clusters. However, no obvious relationship is found between the HOMO−LUMO gap and either the Au/SR ratio or the cluster size for the RS−AuNPs in the transition region (from the homoleptic Au(I) thiolate to the core-stacked nanoparticles). For example, the $Au_{24}(SR)_{20}$ possesses a HOMO−LUMO gap much smaller than that of $Au_{20}(SR)_{16}$ even though both clusters process similar Au_8 cores and Au/SR ratios. A question naturally arises: what factor controls the HOMO−LUMO gap of RS−AuNPs in the transition region from the homoleptic Au(I) thiolate to the core-stacked nanoparticles?

We have computed electronic structures and UV−vis absorption spectra of a series of homoleptic Au(I) thiolate and RS−AuNPs, ranging from $Au_{10}(SR)_{10}$, $Au_{12}(SR)_9^+$, $Au_{20}(SR)_{16}$, $Au_{25}(SR)_{18}^-$ to $Au_{38}(SR)_{24}$. Moreover, absorption spectrum of the nearly 2 nm sized $Au_{102}(SR)_{44}$ in region of 0−0.8 eV is computed (cf. Supporting Information, Figure S4), which is in good agreement with recent experimental and theoretical results.[14b] The computed Kohn−Sham orbital transition modes of $Au_{10}(SR)_{10}$, $Au_{12}(SR)_9^+$, $Au_{20}(SR)_{16}$, $Au_{24}(SR)_{20}$, $Au_{25}(SR)_{18}^-$, $Au_{38}(SR)_{24}$, and $Au_{102}(SR)_{44}$ indicate that the first absorption peak for all clusters is contributed mainly from the HOMO to LUMO excitation. In Figure 5a, we present a trend of HOMO and LUMO energies versus the cluster's composition. We find that all neutral clusters have similar values of HOMO energy except $Au_{20}(SR)_{16}$, which has a large drop (~0.5 eV) in HOMO energy compared with other RS−AuNPs. Hence, the reduction of the HOMO−LUMO gap is largely due to the decrease of LUMO energy.

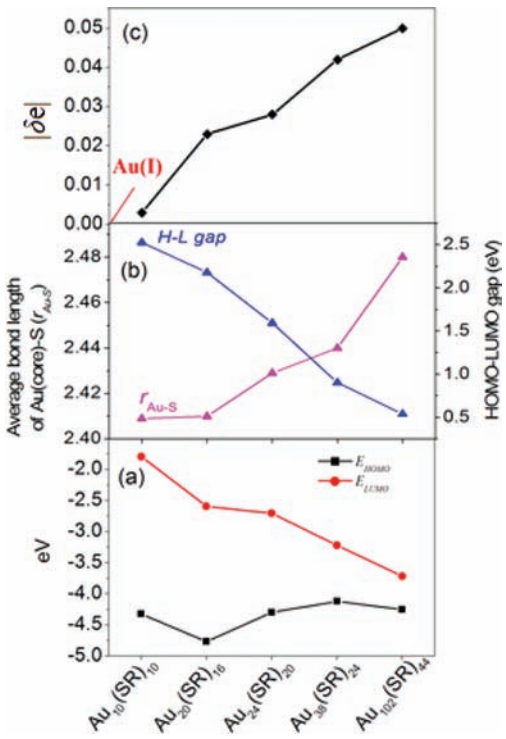

Figure 5. (a) Calculated KS energies of HOMO and LUMO for various RS−AuNPs. (b) A relation between the HOMO−LUMO gap and the average bond length of the Au(core)−S (r_{Au-S}) for RS−AuNPs of different size. The bond length of the Au(core)−S is based on the optimized geometries at the PBE/TZP level. (c) Calculated Hirshfeld charge difference (|δe|) between the charge on Au atom in the staple motifs and that in the core.

To obtain more insights into electronic structures of RS−AuNPs with different compositions, we have performed atom-projected local density (PLDOS) analysis for $Au_{10}(SR)_{10}$, $Au_{12}(SR)_9^+$, $Au_{20}(SR)_{16}$, $Au_{24}(SR)_{20}$, $Au_{25}(SR)_{18}^-$, $Au_{38}(SR)_{24}$, and $Au_{102}(SR)_{44}$ (collected in the Supporting Information, Figure S5). The PLDOS analysis gives rise to different local electronic structures for Au atoms in the Au core and in staple motifs. A constricted 5d band is seen for Au atoms in the staple motifs for all core-stacked clusters, which is in stark contrast to the more broad distribution of the 5d band for Au atoms in the Au cores. This result supports the divide-and-protect scheme.[21] Furthermore, one may find that the Au atoms in the Au core contribute significantly to the HOMO and LUMO, regardless of the cluster size. It is known that the ligand shell can strongly affect electronic structures of the Au core.[19,21−23,62] Here, a general relation between the HOMO−LUMO gap and average bond length of the Au(core)−S is obtained in Figure 5b. Notably, we find that the HOMO−LUMO gap of RS−AuNPs decreases with the increase of average bond length of Au(core)−S. It is believed that the Au atoms in the core and those in staple motifs are in different chemical states, that is, Au(I) and Au(0). With the increase of the bond length between Au(core) and S atom, the interaction between the Au core and staple motifs becomes weaker, from the homeleptic $Au_{10}(SR)_{10}$ to the core-stacked RS−AuNPs. The computed average charge distribution (|δe|) and PLDOS of the 5d orbital of Au atoms in the Au core and staple motifs (see Figure 5c and the Supporting Information, Figure S6) indicated that with the increase of average bond length of Au(core)−S, the difference in |δe| as well as PLDOS (5d) between Au atoms in the staple motif and in the core increases (cf. Figure 5c and Supporting Information, Figure S6). For the homoleptic catenane $Au_{10}(SR)_{10}$, the |δe| and PLDOS (5d) on each Au atom are almost the same, indicating that no distinct Au core is formed, suggesting that all Au atoms are in the Au(I) state. However, with the difference in the |δe| and PLDOS (5d) between Au atoms in the core and staple motifs becoming larger, for example, from $Au_{20}(SR)_{16}$ to $Au_{24}(SR)_{20}$, more Au atoms belong to the metallic Au core, which accounts for the decrease of the HOMO−LUMO gap. Such a trend is also valid for larger-sized RS−AuNPs, such as $Au_{38}(SR)_{24}$ and $Au_{102}(SR)_{44}$, which possess increasingly larger metallic Au core, and a more quickly reduced HOMO−LUMO gap.

4. CONCLUSION

We have predicated atomic structure of a recently synthesized $Au_{24}(SR)_{20}$ cluster by using the classical force-field based divide-and-protect approach. We find that the lowest-energy isomer of $Au_{24}(SR)_{20}$ possesses unique catenane-like $[Au_3(SR)_4]$-$[Au_5(SR)_6]$ staple motifs that have not been reported previously in all known RS−AuNPs. This finding suggests that the appearance of interlocked staple motifs occurs for RS−AuNPs with relatively low Au/SR ratio. The onset of interlocked $[Au_7(SR)_6][Au_5(SR)_5]$ oligomer structures in $Au_{24}(SR)_{20}$ also supports a recently proposed growth mechanism of RS−AuNPs, which suggests that $Au_n(SR)_{n-1}$ oligomers are likely involved in the initial growth of RS−AuNPs.[34] Regarding the Au core, we conclude that, for RS−AuNPs with smaller cluster size and

dx.doi.org/10.1021/ja208559y | J. Am. Chem.Soc. 2012, 134, 3015−3024

relatively low Au/SR ratio (Au/SR < 1.33), the tetrahedron Au_4 unit appears to be a prevalent structural motif, as opposed to the close-packed 13 atom icosahedrons, octahedron, or decahedron structural motifs showing in larger clusters $Au_{25}(SR)_{18}^-$, $Au_{38}(SR)_{24}$, and $Au_{102}(SR)_{44}$, respectively.[8,35] Moreover, we find that, with the increase of interfacial bond length of Au(core)−S, an increasingly larger metallic core is formed in RS−AuNPs, which results in a smaller HOMO−LUMO gap. In closing, the newly developed force-field based divide-and-protect approach can be extended to predict structures of larger-sized RS−AuNPs, which are greatly needed for better understanding of their structure−function relationship.

■ ASSOCIATED CONTENT

Supporting Information

Relative and absolute electronic energies, UV−vis absorption spectra of higher energy isomers (**Iso4**−**Iso10**), the Cartesian coordinate and CD spectra of **Iso1**−**Iso3**, and PLDOS analysis of various RS−AuNPs. This material is available free of charge via the Internet at http://pubs.acs.org.

■ AUTHOR INFORMATION

Corresponding Author

ypnku78@gmail.com; xzeng1@unl.edu

Notes

The authors declare no competing financial interest.

■ ACKNOWLEDGMENTS

Y.P. is supported by the Natural Science Foundation of China (grant no. 21103144) and Academic Leader Program in Xiangtan University (10QDZ34). X.C.Z. is supported by grants from NSF (DMR-0820521, EPS-1010094), ARL (W911NF1020099), and a seed grant by the Nebraska Center for Energy Sciences Research. Discussions with Professors R. Jin, M. Zhu, and C. M. Aikens are appreciated. The authors also thank Professor R. Jin for providing the original data of powder XRD and UV−vis absorption and reviewers' valuable comments.

■ REFERENCES

(1) (a) Whetten, R. L.; Khoury, J. T.; Alvarez, M. M.; Murthy, S.; Vezmar, I.; Wang, Z. L.; Stephens, P. W.; Cleveland, C. L.; Luedtke, W. D.; Landman, U. *Adv. Mater.* **1996**, *8*, 428. (b) Schaaff, T. G.; Shafigullin, M. N.; Khoury, J. T.; Vezmar, K. I.; Whetten, R.; Gullen, W. G.; First, P. N. *J. Phys. Chem. B* **1997**, *101*, 7885. (c) Chen, S.; Ingram, R. S.; Hostetler, M. J.; Pietron, J. J.; Murray, R. W.; Schaaff, T. G.; Khoury, J. T.; Alvarez, M. M.; Whetten, R. L. *Science* **1998**, *280*, 2098. (d) Templeton, A. C.; Wuelfing, W. P.; Murray, R. W. *Acc. Chem. Res.* **2000**, *33*, 27. (e) Sardart, R.; Funston, A. M.; Mulvaney, P.; Murray, R. W. *Langmuir* **2009**, *25*, 13840. (f) Price, R. C.; Whetten, R. L. *J. Am. Chem. Soc.* **2005**, *127*, 13750.

(2) (a) Tsunoyama, H.; Nickut, P.; Negishi, Y.; Al-Shamery, K.; Matsumoto, Y.; Tsukuda, T. *J. Phys. Chem. C* **2007**, *111*, 4153. (b) Chaki, N. K.; Tsunoyama, H.; Negishi, Y.; Sakurai, H.; Tsukuda, T. *J. Phys. Chem. C* **2007**, *111*, 4885. (c) Tsunoyama, H.; Sakurai, H.; Negishi, Y.; Tsukuda, T. *J. Am. Chem. Soc.* **2005**, *127*, 9374. (d) Tsunoyama, H.; Sakurai, H.; Tsukuda, T. *Chem. Phys. Lett.* **2006**, *429*, 528. (e) Liu, Y.; Tsunoyama, H.; Akita, T.; Tsukuda, T. *Chem. Commun.* **2010**, *46*, 550. (f) Liu, Y.; Tsunoyama, H.; Akita, T.; Tsukuda, T. *ACS Catal.* **2011**, *1*, 2.

(3) Lopez-Acevedo, O.; Kacprzak, K. A.; Akola, J.; Häkkinen, H. *Nat. Chem.* **2010**, *2*, 329.

(4) Huang, X.; El-Sayed, I. H.; Qian, W.; El-Sayed, M. A. *J. Am. Chem. Soc.* **2006**, *128*, 2115.

(5) Cao, Y. C.; Jin, R.; Nam, J.; Thaxton, C. S.; Mirkin, C. A. *J. Am. Chem. Soc.* **2003**, *125*, 14676.

(6) (a) Jin, R. *Nanoscale* **2010**, *2*, 343. (b) Zhu, Y.; Qian, H.; Drake, B. A.; Jin, R. *Angew. Chem., Int. Ed.* **2010**, *49*, 1295. (c) Zhu, Y.; Qian, H.; Zhu, M.; Jin, R. *Adv. Mater.* **2010**, *22*, 1915. (d) Zhu, Y.; Wu, Z.; Cayathri, G. C.; Qian, H.; Gil, R. R.; Jin, R. *J. Catal.* **2010**, *271*, 155.

(7) Parker, J. F.; Fields-Zinna, C. A.; Murray, R. W. *Acc. Chem. Res.* **2010**, *43*, 1289.

(8) Dass, A. *J. Am. Chem. Soc.* **2009**, *131*, 11666.

(9) (a) Qian, H.; Jin, R. *Nano Lett.* **2009**, *9*, 4083. (b) Zhu, M.; Qian, H.; Jin, R. *J. Am. Chem. Soc.* **2009**, *131*, 7220. (c) Zhu, M.; Qian, H.; Jin, R. *J. Phys. Chem. Lett.* **2010**, *1*, 1003. (d) Jin, R.; Qian, H.; Wu, Z.; Zhu, Y.; Zhu, M.; Mohanty, A.; Garg, N. *J. Phys. Chem. Lett.* **2010**, *1*, 2903. (e) Qian, H.; Jin, R. *Chem. Mater.* **2011**, *23*, 2209. (f) Qian, H.; Zhu, Y.; Jin, R. *J. Am. Chem. Soc.* **2010**, *132*, 4583. (g) Qian, H.; Eckenhoff, W. T.; Zhu, Y.; Pintauer, T.; Jin, R. *J. Am. Chem. Soc.* **2010**, *132*, 8280. (i) Wu, Z.; MacDonald, M. A.; Chen, J.; Zhang, P.; Jin, R. *J. Am. Chem. Soc.* **2011**, *133*, 9670.

(10) Negishi, Y.; Takasugi, Y.; Sato, S.; Yao, H.; Kimura, K.; Tsukuda, T. *J. Am. Chem. Soc.* **2004**, *126*, 6518.

(11) Schaaff, T. G.; Whetten, R. L. *J. Phys. Chem. B* **2000**, *104*, 2630.

(12) (a) Ramakrishna, G.; Varnavski, O.; Kim, J.; Lee, D.; Goodson, T. *J. Am. Chem. Soc.* **2008**, *130*, 5032. (b) Varnavski, O.; Ramakrishna, G.; Kim, J.; Lee, D.; Goodson, T. *J. Am. Chem. Soc.* **2010**, *132*, 16.

(13) Wang, Z. W.; Toikkanen, O.; Yin, F.; Li, Z. Y.; Quinn, B. M.; Palmer, R. E. *J. Am. Chem. Soc.* **2010**, *132*, 2854.

(14) (a) Jadzinsky, P. D.; Calero, G.; Ackerson, C. J.; Bushnell, D. A.; Kornberg, R. D. *Science* **2007**, *318*, 430. (b) Levi-Kalisman, Y.; Jadzinsky, P. D.; Kalisman, N.; Tsunoyama, H.; Tsukuda, T.; Bushnell, D. A.; Kornberg, R. D. *J. Am. Chem. Soc.* **2011**, *133*, 2976.

(15) (a) Heaven, M. W.; Dass, A.; White, P. S.; Holt, K. M.; Murray, R. W. *J. Am. Chem. Soc.* **2008**, *130*, 3754. (b) Zhu, M.; Aikens, C. M.; Hollander, F. J.; Schatz, G. C.; Jin, R. *J. Am. Chem. Soc.* **2008**, *130*, 5883.

(16) Akola, J.; Walter, M.; Whetten, R. L.; Häkkinen, H.; Grönbeck, H. *J. Am. Chem. Soc.* **2008**, *130*, 3756.

(17) (a) Jiang, D.; Whetten, R. L.; Luo, W.; Dai, S. *J. Phys. Chem. C* **2009**, *113*, 17291. (b) Jiang, D. *Chem.—Eur. J.* **2011**, *17*, 12289.

(18) Jiang, D.; Chen, W.; Whetten, R. L.; Chen, Z. *J. Phys. Chem. C* **2009**, *113*, 16983.

(19) Pei, Y.; Gao, Y.; Shao, N.; Zeng, X. C. *J. Am. Chem. Soc.* **2009**, *131*, 13619.

(20) Jiang, D.; Tiago, M. L.; Luo, W.; Dai, S. *J. Am. Chem. Soc.* **2008**, *130*, 2777.

(21) Häkkinen, H.; Walter, M.; Grönbeck, H. *J. Phys. Chem. B* **2006**, *110*, 9927.

(22) Pei, Y.; Gao, Y.; Zeng, X. C. *J. Am. Chem. Soc.* **2008**, *130*, 7830.

(23) Lopez-Acevedo, O.; Tsunoyama, H.; Tsukuda, T.; Häkkinen, H.; Aikens, C. M. *J. Am. Chem. Soc.* **2010**, *132*, 8210.

(24) Jiang, D.; Walter, M.; Akola, J. *J. Phys. Chem. C* **2010**, *114*, 15883.

(25) Lopez-Acevedo, O.; Akola, J.; Whetten, R. L.; Grönbeck, H.; Häkkinen, H. *J. Phys. Chem. C* **2009**, *113*, 5305.

(26) (a) Walter, M.; Akola, J.; Lopez-Acevedo, O.; Jadzinsky, P. D.; Calero, G.; Ackerson, C. J.; Whetten, R. L.; Grönbeck, H.; Häkkinen, H. *Proc. Natl. Acad. Sci. U.S.A.* **2008**, *105*, 9157. (b) Häkkinen, H. *Chem. Soc. Rev.* **2008**, *37*, 1847.

(27) Reimers, J. R.; Wang, Y.; Cankurtaran, B. O.; Ford, M. J. *J. Am. Chem. Soc.* **2010**, *132*, 8378.

(28) Han, Y.-K.; Kim, H.; Jung, J.; Choi, Y. C. *J. Phys. Chem. C* **2010**, *114*, 7548.

(29) Brust, M.; Walker, M.; Bethell, D.; Schiffrin, D. J.; Whyman, R. *J. Chem. Soc., Chem. Commum.* **1994**, 801.

(30) Alvarez, M. M.; Khoury, J. T.; Schaaf, T. G.; Schafifulin, M.; Vezmar, I.; Whetten, R. L. *Chem. Phys. Lett.* **1997**, *266*, 91.

(31) Negishi, Y.; Nobusada, K.; Tsukuda, T. *J. Am. Chem. Soc.* **2005**, *127*, 5261.

(32) Goulet, P. J. G.; Lennox, R. B. *J. Am. Chem. Soc.* **2010**, *132*, 9582.

(33) Wu, Z.; MacDonald, M. A.; Chen, J.; Zhang, P.; Jin, R. *J. Am. Chem. Soc.* **2011**, *133*, 9670.
(34) Barngrover, B. M.; Aikens, C. M. *J. Phys. Chem. Lett.* **2011**, *2*, 990.
(35) Dharmaratne, A. C.; Krick, T.; Dass, A. *J. Am. Chem. Soc.* **2009**, *131*, 13604.
(36) Gao, Y.; Shao, N.; Zeng, X. C. *ACS Nano* **2008**, *2*, 1497.
(37) Wiseman, M. R.; Marsh, P. A.; Bishop, P. T.; Brisdon, B. J.; Mahon, M. F. *J. Am. Chem. Soc.* **2000**, *122*, 12598.
(38) Hartke, B. *J. Phys. Chem.* **1993**, *97*, 9973.
(39) Xiang, H.; Wei, S.-H.; Gong, X. *J. Am. Chem. Soc.* **2010**, *132*, 7355.
(40) Kirkpatrick, S.; Gelatt, C. D.; Vecchi, M. P. *Science* **1983**, *220*, 671.
(41) (a) Wales, D. J.; Doye, J. P. K. *J. Phys. Chem. A* **1997**, *101*, 5111. (b) Yoo, S.; Zeng, X. C. *Angew. Chem., Int. Ed.* **2005**, *44*, 1491.
(42) Sutton, A. P.; Chen, J. *Philos. Mag. Lett.* **1990**, *61*, 139.
(43) Goel, S.; Velizhanin, K. A.; Piryatinski, A.; Tretiak, S.; Ivanov, S. A. *J. Phys. Chem. Lett.* **2010**, *1*, 927.
(44) Guliamov, O.; Frenkel, A. I.; Menard, L. D.; Nuzzo, R. G.; Kronik, L. *J. Am. Chem. Soc.* **2007**, *129*, 10978.
(45) Delley, B. *J. Chem. Phys.* **1990**, *92*, 508; *J. Chem. Phys.* **2003**, *113*, 7756DMol^3 4.3 is available from Accelrys.
(46) *ADF 2010.01*, SCM, Theoretical Chemistry; Vrije Universiteit: Amsterdam, The Netherlands; http://www.scm.com.
(47) Frisch, M. J.; et al. *Gaussian 09*, Revision A.02; Gaussian, Inc.: Wallingford, CT, 2009.
(48) Perdew, J. P.; Burke, K.; Ernzerhof, M. *Phys. Rev. Lett.* **1996**, *77*, 3865.
(49) Staroverov, V. N.; Scuseria, G. E.; Tao, J.; Perdew, J. P. *J. Chem. Phys.* **2003**, *119*, 12129.
(50) (a) Zhao, Y.; Truhlar, D. G. *J. Phys. Chem. A* **2006**, *110*, 13126. (b) Zhao, Y.; Truhlar, D. G. *J. Chem. Phys.* **2006**, *125*, 194101.
(51) (a) Head-Gordon, M.; Pople, J. A.; Frisch, M. J. *Chem. Phys. Lett.* **1988**, *153*, 503. (b) Frisch, M. J.; Head-Gordon, M.; Pople, J. A. *Chem. Phys. Lett.* **1990**, *166*, 275.
(52) Mantina, M.; Valero, R.; Truhlar, D. G. *J. Chem. Phys.* **2009**, *131*, 064706.
(53) Chaki, N. K.; Negishi, Y.; Tsunoyama, H.; Schichibu, Y.; Tsukuda, T. *J. Am. Chem. Soc.* **2008**, *130*, 8608.
(54) (a) Shao, N.; Pei, Y.; Gao, Y.; Zeng, X. C. *J. Phys. Chem. A* **2009**, *113*, 629. (b) Grönbeck, H.; Walter, M.; Häkkinen, H. *J. Am. Chem. Soc.* **2006**, *128*, 10268.
(55) Clemenger, K. *Phys. Rev. B* **1985**, *32*, 1359.
(56) Aikens, C. M. *J. Phys. Chem. C* **2008**, *112*, 19797.
(57) Provorse, M. R.; Aikens, C. M. *J. Am. Chem. Soc.* **2010**, *132*, 1302.
(58) Zeller, E.; Beruda, H.; Schmidbaur, H. *Inorg. Chem.* **1993**, *32*, 3203.
(59) Briant, C. E.; Hall, K. P.; Mingos, D. M. P.; Wheeler, A. C. *J. Chem. Soc., Dalton Trans.* **1986**, 687.
(60) Negishi, Y.; Nobusada, K.; Tsukuda, T. *J. Am. Chem. Soc.* **2005**, *127*, 5261.
(61) Zhang, Y.; Shuang, S.; Dong, C.; Lo, C. K.; Paau, M. C.; Choi, M. M. F. *Anal. Chem.* **2009**, *81*, 1676.
(62) Briant, C. E.; Tobald, B. R. C.; White, J. W.; Bell, L. K.; Mingos, D. M. P. *Chem. Commun.* **1981**, 201.